Archives of Biochemistry and Biophysics 748 (2023) 109772

Contents lists available at ScienceDirect

Archives of Biochemistry and Biophysics

journal homepage: www.elsevier.com/locate/yabbi

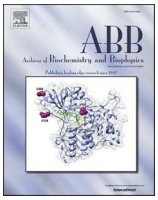

Dihydropyrmidine dehydrogenase from *Escherichia coli*: Transient state analysis reveals both reductive activation prior to turnover and diminished substrate effector roles relative to the mammalian form

Tyler B. Alt, Matthew R. Hoag, Graham R. Moran *

Department of Chemistry and Biochemistry, 1068 W Sheridan Rd, Loyola University Chicago, Chicago, IL 60660, USA

A B S T R A C T

Dihydropyrimidine dehydrogenase (DPD) is an enzyme that uses an elaborate architecture to catalyze a simple net reaction: the reduction of the vinylic bond of uracil and thymine. Known DPDs have two active sites separated by approximately 60 Å. One active site has an FAD cofactor and binds NAD(P) and the other has an FMN cofactor and binds pyrimidines. The intervening distance is spanned by four Fe_4S_4 centers that act as an electron conduit. Recent advancements with porcine DPD have revealed unexpected chemical sequences where the enzyme undergoes reductive activation by transferring two electrons from NADPH to the FMN via the FAD such that the active form has the cofactor set FAD•4(Fe_4S_4)•$FMNH_2$. Here we describe the first comprehensive kinetic investigation of a bacterial form of DPD. Using primarily transient state methods, DPD from *E. coli* (EcDPD) was shown to have a similar mechanism to that observed with the mammalian form in that EcDPD is observed to undergo reductive activation before pyrimidine reduction and displays half-of-sites activity. However, two distinct aspects of the EcDPD reaction relative to the mammalian enzyme were observed that relate to the effector roles for substrates: (i) the enzyme will rapidly take up electrons from NADH, reducing a flavin in the absence of pyrimidine substrate, and (ii) the activated form of the enzyme can become fully oxidized by transferring electrons to pyrimidine substrates in the absence of NADH.

1. Introduction

The catabolism of pyrimidines is initiated by reduction of the 5,6-vinylic bond using electrons from NAD(P)H (Scheme 1) and the reduction of the pyrimidine substrate is favored by 10–20 kj/mol [1]. This simple reaction is catalyzed by dihydropyrimidine dehydrogenase (DPD), an enzyme with a complex cofactor set comprised of two flavins (FAD and FMN) and four iron-sulfur centers (Fe_4S_4).

Structures of mammalian DPD indicate that these cofactors are arranged to form an electron conduit that bridges NAD(P)H, bound adjacent to the FAD, to the pyrimidine, that binds adjacent to the FMN (Fig. 1) [2]. The porcine form of DPD has been studied extensively [1–9]. The mammalian enzyme is a functional homodimer in that the four iron-sulfur centers of any one conduit include two from each subunit. It has recently been shown that the mammalian enzyme exhibits numerous unexpected mechanistic sequences. Principal among these is that prior to catalytic turnover the enzyme is observed to take up two electrons from NADPH in a reductive activation process that requires pyrimidine substrate as an effector. The electrons are acquired at the FAD but traverse the protein to reside on the FMN so that the active cofactor set is FAD•4(Fe_4S_4)•$FMNH_2$ [8]. Only in the presence of NADPH will this activated form of the enzyme reduce pyrimidine substrates [1], the NADPH being utilized to reinstate the active cofactor set with pyrimidine reduction in what amounts to reductive re-activation. The mammalian enzyme also exhibits alternating sites behavior whereby one subunit activates and turns over before catalytic engagement of the second subunit [9]. These unusual sequences suggest both inter-active site and inter-subunit contingencies that govern catalysis.

In the study presented here we characterize the kinetic behavior of DPD from *Escherichia coli* (EcPDP). The structure of EcDPD has not been solved, but the enzyme is expressed from two genes, *preT* and *preA*, indicating that its structure differs from mammalian forms [10]. These yield two subunits, whose primary structures are predicted to form PreT that houses the FAD and two Fe_4S_4 iron-sulfur centers and PreA containing the FMN and two Fe_4S_4 iron-sulfur centers (Fig. 1). This altered arrangement of subunits may exhibit catalytic sequences that differ from those observed for mammalian forms of the enzyme. Specifically, it is unclear whether reductive (re)activation and/or alternating sites play a role in catalysis for all forms of the enzyme. We have characterized EcDPD cofactor content, pyrimidine ligand binding, and the kinetics of the reductive half-reaction and single turnover using anaerobic steady-state and transient-state measurements. The data obtained

* Corresponding author.
E-mail address: gmoran3@luc.edu (G.R. Moran).

https://doi.org/10.1016/j.abb.2023.109772
Received 9 August 2023; Received in revised form 27 September 2023; Accepted 28 September 2023
Available online 9 October 2023

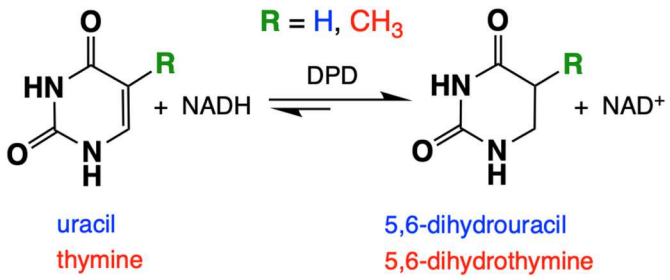

Scheme 1. The Reaction Catalyzed by Dihydropyrimidine Dehydrogenase.

suggest that EcDPD is similar to the mammalian enzyme in that it undergoes reductive activation and exhibits half-of-sites behavior, but differs in that it has no effector response to pyrimidine binding and has a modified effector role for NADH. During catalysis, electrons flow from NADH to reductively activate the enzyme and subsequently to reduce the pyrimidine. However, unlike the mammalian enzyme, when NADH is exhausted EcDPD delivers the residual two electrons to the pyrimidine substrate and returns to the FAD•4(Fe_4S_4)•FMN state. However, it does this reoxidation at a rate approximately one-third of that observed in the presence of NADH.

2. Materials and methods

2.1. Materials and quantitation

The Miller formulation of lysogeny broth (LB) was purchased from RPI. Competent *E. coli* BL21 (DE3) cells were purchased from New England Biolabs. Fe(SO_4), uracil, thymine, flavin adenine dinucleotide (FAD), imidazole, 2-mercaptoethanol (BME), tryptophan, and triethylamine (TEA) were purchased from Acros. Ampicillin, dihydrouracil (DHU), and dihydrothymine (DHT) were purchased from Alfa Aesar. Oxidized nicotinamide adenine dinucleotide (NAD^+) was purchased from Amresco. TALON Superflow resin was purchased from Cytiva. Isopropyl-ß-D-thiogalactopyranoside (IPTG), glycerol, Na_2SO_4, sodium dodecyl sulfate (SDS), ethylenediaminetetraacetic acid (EDTA), NH_4Ac, methanol, NaCl, trichloroacetic acid (TCA), and acetonitrile were purchased from Fisher. Monopotassium phosphate was purchased from HiMedia. Glucose oxidase and reduced nicotinamide adenine dinucleotide (NADH) were purchased from Millipore-Sigma. Ferene-S and NaOH wer purchased from Sigma-Aldrich. Glucose was purchased from Spectrum. Flavin mononucleotide (FMN) was purchased from TCI. Nitric acid was purchased from VWR.

Where possible, concentrations were determined based on the following extinction coefficients: EcDPD, ε_{445} = 71,000 $M^{-1}cm^{-1}$ (see below); uracil, ε_{260} = 8,200 $M^{-1}cm^{-1}$ [11]; thymine, ε_{264} = 7,860 $M^{-1}cm^{-1}$ [12]; dihydrouracil, ε_{225} = 1,280 $M^{-1}cm^{-1}$ (determined by weight); dihydrothymine, ε_{225} = 1,670 $M^{-1}cm^{-1}$ (determined by weight); NAD^+, ε_{260} = 17,800 $M^{-1}cm^{-1}$ [13]; NADH, ε_{340} = 6,220 $M^{-1}cm^{-1}$ [14], ScOYE3, ε_{464} = 10,300 $M^{-1}cm^{-1}$ [15]. All other concentrations were defined by weight for solids or using the nominal concentration provided by the manufacturer for liquids.

2.2. EcDPD structural prediction

The structure of each EcDPD subunit was predicted using the AlphaFold Protein Structure Database in conjunction with the structure of *Sus scrofa* DPD (SsDPD) that was previously determined by X-ray crystallographic methods [2]. AlphaFold was used to generate structural predictions of the PreA (UniProt A0A7A3AVK3) and PreT (UniProt A0A4D3QRF9) subunits. Upon visual inspection, portions of the predicted structures appeared similar to structures of porcine DPD (SsDPD). The similarities permitted the use of SsDPD as a scaffold to reconstruct a biological assembly prediction for EcDPD. The PreA subunit was aligned with domain IV of SsDPD and the PreT subunit was aligned with domain II/III of SsDPD [2,16,17].

2.3. Expression and purification

The genes for EcDPD (*preA* and *preT*) were synthesized by Genscript, Inc. (Piscataway, NJ). The codon bias of both genes was optimized for expression in *E. coli*. Both genes were subcloned into the plasmid pETDuet-1, yielding a construct that expresses both subunits of EcDPD with PreA fused to the sequence for a *C*-terminal 6-His tag. The *preT* gene was subcloned into the *Nco*I and *Hin*dIII sites and the *preA* gene was subcloned into the *Nde*I and *Xho*I sites. The resulting plasmid, pEcDPD, was transformed into competent *E. coli* BL21 (DE3) cells and spread onto LB agar plates that included 100 μg/mL ampicillin. Individual colonies were used to inoculate cultures consisting of ~20 mL of sterile LB broth with 100 μg/mL ampicillin. Cells were grown at 37 °C until turbidity was first observed and aliquoted into 600 μL subsamples, mixed with 0.22 μm filtered 50 % glycerol to a final concentration of 20 % and stored at −80 °C. To express EcDPD, cell stocks were thawed and spread on LB agar plates containing 100 μg/mL ampicillin. Plates were incubated at 37 °C for 14–16 h. Cell lawns were then resuspended using ~5 mL of warm LB and used to inoculate 2-L baffled Erlenmeyer flasks each containing 1 L of LB broth and 100 μg/mL ampicillin. The cultures were incubated at 37 °C with shaking at 220 rpm and grown to an optical density of 0.6 at 600 nm before the temperature was lowered to 25 °C and allowed to equilibrate for 1 h. Once cooled, expression was induced with 100 μM IPTG, and 200 μM Fe(SO_4) and 1 mM $Na_2(SO_4)$ was added.

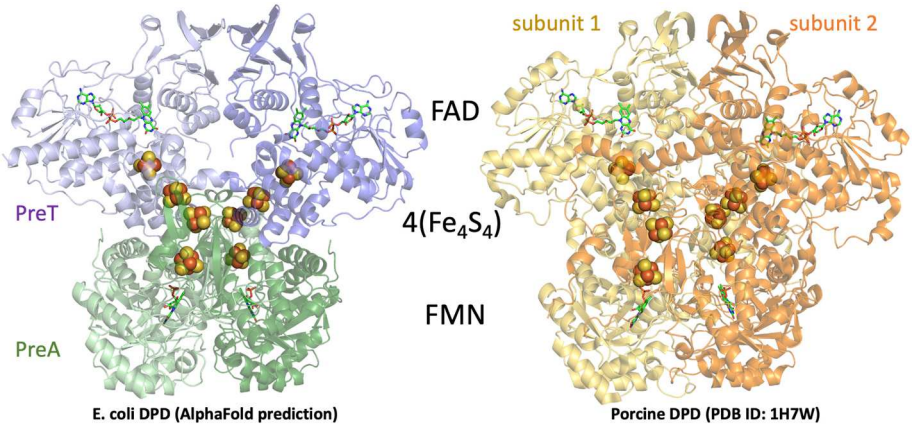

Fig. 1. AlphaFold predicted structure of EcDPD compared to the structure of mammalian DPD. Cofactors for EcDPD are positioned based on structural alignment to the mammalian structure shown to the right.

The cultures were maintained at 25 °C with shaking at 220 rpm for 22 h prior to harvesting by centrifugation at 3,500 g for 35 min. The supernatant was discarded, and the cells were resuspended in 20 mL per liter of culture of ice-cold buffer A (30 mM KPi, 100 mM NaCl, 10 mM imidazole, 2 mM BME, pH 7.4). The cell suspension was transferred to a stainless-steel beaker that was placed in an ice and water slurry. The cells were lysed by sonication at 40 W using 4 bursts of 2 min with 2–3 min between each using a Branson sonifier. The temperature was monitored to ensure the temperature did not exceed 10 °C. Lysed cells were centrifuged at 10,000 g for 45 min to remove cellular debris prior to loading onto a 10 mL BD TALON column pre-equilibrated with buffer A. The column was washed with 100 mL of buffer A prior to eluting the enzyme with a 400 mL linear gradient of 0–100 % buffer B (30 mM KPi, 100 mM NaCl, 300 mM Imidazole, 2 mM BME, pH 7.4) collecting 5 mL fractions. The first major peak was collected, and buffer exchanged and concentrated into buffer C (30 mM KPi, 2 mM BME, pH 7.4) for storage using centrifugal 15 mL 10 kDa cutoff filters.

2.4. Determination of cofactor occupancy in EcDPD

Cofactor occupancy was established by quantitation of flavins and ferrous iron for the same sample of purified EcDPD. High pressure liquid chromatography (HPLC) analysis verified equal loading of the FAD and FMN cofactors. A UV–Vis spectrum was measured for a sample of EcDPD, and the sample was subsequently incubated at 70 °C for 1 h in the presence of 0.2 % SDS, 2 mM BME and 5 mM EDTA. The sample was cooled to 4 °C and diluted two-fold into 1 M potassium phosphate, pH 6.5, to precipitate the SDS. The sample was centrifuged at 10,000 g for 15 min to remove both the SDS and denatured protein. The supernatant was injected onto a reverse phase HPLC column (Waters XBridge C18, 5 μm, 4.6 × 250 mm) preequilibrated with 5 mM ammonium acetate in 15 % methanol, pH 6.5. The column was coupled to a Shimadzu Prominence HPLC system. Elution was performed isocratically in the same mobile phase at 1 mL/min. Elution of the flavins was detected at 380 nm. The resulting peak areas were compared with a standard curve generated under the same conditions using samples of known FAD and FMN concentrations.

To determine the amount of iron present in the purified EcDPD, the Ferene-S assay described by Hedayati et al. was utilized [18]. A 1× working solution of 5 mM Ferene-S, 0.2 M ascorbic acid, and 0.4 M ammonium acetate, pH 4.3, was prepared and stored at −20 °C prior to use. From the same sample used in the flavin cofactor analysis above, 10 μL was mixed with 100 μL of concentrated nitric acid and incubated for 90 min at 70 °C. The sample was cooled to room temperature and neutralized with 160 μL of 10 M NaOH. The total volume was brought to 1 mL by the addition of 730 μL of the 1× Ferene-S solution, and the sample was incubated at room temperature in the dark for ~16 h. After the incubation period, the UV–Vis spectrum of the sample was measured, and the concentration of ferrous iron was determined using the extinction coefficient of 35,200 $M^{-1}cm^{-1}$ at 595 nm for the Ferene-S/Fe^{2+} complex [19].

2.5. Calculation of the extinction coefficient of EcDPD

The verification of the expected ratio of all cofactors in the purified sample of EcDPD allows for an extinction coefficient to be calculated using the UV–Vis spectrum and the concentration of flavins as determined by the HPLC and chelator analyses described above. Given that the FAD and FMN cofactors were found to be in equivalent molar concentrations, and that each catalytically active dimer of EcDPD contains one FAD and one FMN, the concentration of enzyme in a given sample will be equal to the concentration of one half of the total concentration of flavin cofactors. Using this method, the extinction coefficient for EcDPD PreAT protomer was determined to be 71,000 $M^{-1}cm^{-1}$ at 445 nm.

2.6. Steady-state analysis of EcDPD

Steady-state kinetic analysis of EcDPD used the absorption changes associated with oxidation of NADH as an observational handle. For aerobic measurements, a sample of EcDPD (710 nM) was mixed with a solution containing 50 μM NADH and varied concentrations of pyrimidine substrate (0–320 μM) using a stopped-flow spectrophotometer. Anaerobic steady-state measurements with NADH were undertaken similarly. A sample of EcDPD (650 nM) was mixed with a solution containing varied concentrations of NADH (0–144 μM) and either 150 μM uracil or 150 μM O_2 as the oxidant substrate. A similar procedure was repeated for the anaerobic steady-state kinetics where the concentration of both pyrimidine substrates was varied. A sample of EcDPD (990 nM) was mixed anaerobically with a solution of 100 μM NADH and varied concentrations of either uracil (0–320 μM) or thymine (0–320 μM).

For all assays the reaction was monitored at 340 nm for 100 s and the initial rate was determined from the linear part of the curve, between 10 and 20 s. Initial rates were plotted against concentration of pyrimidine or NADH and fit to the Michaelis-Menten equation (Equation (1)) using Kaleidagraph software. Additionally, apparent k_{cat}/K_M (TN_{app}/K_M) values were determined for each substrate by fitting the data to a variation of the Michaelis-Menten equation (Equation (2)). In these equations Av. TN_{app} refers to the apparent average turnover number at a given concentration of substrate. This axis label was used in place of the $V_0/[e]$ label as an acknowledgment that the fraction of active enzyme was not established.

$$Av.\ TN_{app} = \frac{TN_{app}[S]}{K_M + [S]} \quad \text{Equation 1}$$

$$Av.\ TN_{app} = \frac{TN_{app}[S]}{TN_{app}/(TN_{app}/K_M) + [S]} \quad \text{Equation 2}$$

2.7. Determination of dissociation constants

The dissociation constants for EcDPD•pyrimidine complexes were determined using the perturbation of the absorption spectrum that occurs with binding. The enzyme was found to be unstable in the presence of high concentrations of substrate for extended periods of time, which necessitated the use of a method that minimized error arising from the loss of natively folded enzyme. A solution of EcDPD between 0.5 and 1 μM was separated into 1 mL aliquots. To each, 10 μL of a solution containing the pyrimidine substrate (0–64 μM after dilution) was added and following a 5-min incubation, the UV–Vis absorption spectrum was recorded. Difference spectra were determined by subtracting the unliganded enzyme spectrum from all other spectra. The largest spectral perturbation as a result of binding was observed at 503–507 nm. This spectral change (ΔAbs for a specified wavelength) was plotted against the total concentration of ligand ([L]) and fit to the quadratic form of the single-site binding equation (Equation (3)) using Kaleidagraph software to determine the dissociation constant (K_d) of the ligand to the enzyme-ligand complex.

$$\Delta Abs = \frac{([L] + \Delta Abs_{max} + K_d) - \sqrt{([L] + \Delta Abs_{max} + K_d)^2 - (4[L]\ \Delta Abs_{max})}}{2} \quad \text{Equation 3}$$

2.8. Methods for anaerobic analyses

Anaerobic observations were made using previously published protocols [20]. Enzyme samples were prepared in a glass tonometer and included 1 mM D-glucose. A side arm of the tonometer contained 1 unit of glucose oxidase per milliliter of the enzyme sample. The tonometer was made anaerobic by 30 cycles of alternating argon (5 psi) and vacuum. Upon completion of the cycling, the enzyme sample was allowed to

flow into the side arm, mixing with the glucose oxidase solution. The tonometer was immediately loaded onto a stopped-flow spectrophotometer (TgK Scientific) that had previously been scrubbed of oxygen using a solution of glucose and glucose oxidase. Substrate samples also contained 1 mM glucose and were made anaerobic by sparging with argon for 5 min, 1 U/mL glucose oxidase was added immediately after sparging. All transient state kinetic analyses were carried out in 30 mM KPi, pH 7.4, at 20 °C. Each final data set is the average of at least three observations. To provide maximum resolution of all phases, data was collected on multiple time frames and spliced together at the upper limit of the shorter time frame. All reported concentrations are post mixing unless stated otherwise.

2.9. EcDPD reductive half reaction

The reductive half reaction of EcDPD was characterized using transient-state kinetic methods. A sample of EcDPD (4.7 μM) was made anaerobic as described above and mounted onto a stopped-flow spectrophotometer configured for photomultiplier detection. The sample was mixed with varying concentrations of NADH (0–640 μM) and the reaction was observed at two wavelengths, 340 and 445 nm, for two time frames, 0.0012–0.2 and 0.0012–10 s. The resulting traces were fit to a linear combination of three exponentials (Equation (4)) using Kaleidagraph Software. In this equation, C is the endpoint absorbance at a specified wavelength, ΔA is the amplitude of phase n, k_{obsn} is the observed rate constant of phase n, and t is the time in seconds. The dependence of the observed rate constant for the first phase was fit to Equation (5) to define the limiting rate of reduction (k_{red}) and the apparent K_d for NADH (K_{NADH}). The reaction was also monitored using charge-coupled device (CCD) detection to obtain time-resolved spectra. A sample of EcDPD (14.8 μM) was mixed with NADH (76.4 μM) anaerobically using a stopped-flow spectrophotometer. The reaction was monitored between 300 and 800 nm from 0.0016 to 10 s. The time-resolved spectra were then fit to a two-step irreversible model and deconvoluted using the singular value decomposition (SVD) routine in KinTek Explorer.

$$\mathrm{Abs} = C + \left(\sum_{n=1}^{x} \Delta A_n \left(e^{-k_{obsn} t} \right) \right) \quad \text{Equation 4}$$

$$k_{obs} = \frac{k_{red}[NADH]}{K_{NADH} + [NADH]} \quad \text{Equation 5}$$

2.11. EcDPD single turnover

The reaction between EcDPD and its substrates was characterized with saturating pyrimidine and limiting NADH using transient-state kinetic methods. A sample of EcDPD (4.6 μM) was made anaerobic as described above and mounted onto a stopped-flow spectrophotometer equipped with a photomultiplier detector. Substrate samples contained either uracil (200 μM) and NADH (3.3 μM) or thymine (200 μM) and NADH (3.5 μM). The enzyme and substrate samples were mixed and data was collected at two wavelengths, 445 and 340 nm, for two time frames, 0.0012–0.2 and 0.0012–100 s. The resulting data from 445 nm were fit to a linear combination of two exponentials and those from 340 nm to three exponentials (Equation (4)) using Kaleidagraph Software. The reaction was also monitored using CCD detection to obtain time-resolved spectra. A sample of EcDPD (7.8 μM) was mixed with limiting NADH (6.1 μM) and saturating pyrimidine (uracil or thymine, 200 μM) anaerobically using a stopped-flow spectrophotometer. The reaction was monitored between 300 and 800 nm from 0.0016 to 1.6 and 0.0016–156 s. The time-resolved spectra were then fit to a three-step irreversible model and deconvoluted using the SVD routine in KinTek Explorer.

2.10. EcDPD reductive half reaction with NADH and dihydrouracil

The reductive half reaction of EcDPD was observed in the presence of both NADH and dihydrouracil. A sample of EcDPD (4.7 μM) was made anaerobic as described above and mounted onto a stopped flow spectrophotometer equipped with photomultiplier detection. Substrate samples were also made anaerobic and contained 101 μM NADH and varied concentrations of dihydrouracil (0–500 μM). Enzyme and substrate samples were mixed, and the reaction was monitored at 445 nm for two timeframes, 0.0012–0.2 and 0.0012–10 s.

2.12. Rapid mixing acid quench

The reaction catalyzed by EcDPD was characterized under single turnover conditions using a rapid quench flow instrument (RQF-73, TgK Scientific). Prior to the start of the experiment, the RQF was scrubbed of oxygen using a buffered solution of 1 mM glucose and 1 U/mL glucose oxidase for 4 h. The concentrations reported for the rapid quench experiment are initial concentrations. A sample of EcDPD (26 μM) was made anaerobic as described above and mounted onto the RQF instrument. A substrate solution containing 26 μM NADH and 300 μM thymine, and a quench solution containing 1 M TCA and 1 mM EDTA were made anaerobic by sparging and loaded onto the instrument. The substrate solution also contained 300 μM tryptophan, which served as an inert internal standard. The enzyme and substrate solutions were mixed 1:1 and allowed to react for a defined period (0.004–100 s) before being mixed with the quench solution in a 1:1 ratio. Samples were promptly retrieved from the instrument and placed on ice for a minimum of 15 min, after which they were centrifuged for 15 min at 10,000 g to remove the precipitated protein. The supernatant was collected and stored at −80 °C overnight. Each age time was performed in duplicate. A time zero point was also generated using the same method with anaerobic buffer in place of the enzyme sample. Samples collected from the RQF were analyzed using HPLC. A 20 μL subsample was injected onto a C18 reverse phase column (Waters XBridge C18, 5 μm, 4.6 × 250 mm) that had been preequilibrated with 10 mM ammonium acetate, 1 % acetonitrile, and 15 mM triethylamine, pH 6.5. Elution was performed isocratically at 1 mL/min in the same mobile phase. The elution was monitored at 220 and 260 nm. Standard curves were generated under the same conditions for NAD^+ and thymine. All peak areas derived from the HPLC analysis were normalized based on the peak area of the tryptophan internal standard.

2.13. Validation of anaerobic conditions within the quench instrument

Prior to undertaking the acid quench single turnover experiment with EcDPD, a method to validate the anaerobic environment within the quench instrument was developed. Due to the Tefzel capillary purge lines of the instrument being open to the atmosphere, great care must be taken at all times to ensure there is no significant oxygen ingress to the system. Old yellow enzyme from *Saccharomyces cerevisiae* (ScOYE-3) was used as it is known to reduce molecular oxygen with electrons derived from NADH.

The gene for ScOYE-3 was codon optimized for expression in *E. coli* and the pET-28a derived plasmid was ordered from Enzymax. Competent *E. coli* BL21 (DE3) cells were transformed, and cells were plated on LB agar (50 mg/mL kanamycin). Cultures were incubated at 37 °C overnight, and individual colonies were selected and grown in LB at 37 °C with shaking at 220 rpm until growth reached early log phase (about 3 h). Cell stocks were produced by dividing into aliquots, adding 0.22 μM filtered glycerol to a final concentration of 20 %, and storing at −80 °C.

To express ScOYE-3, the 1 mL cell stocks were thawed and spread on LB Agar plates containing 50 mg/mL kanamycin. Plates were incubated at 37 °C for 14–16 h. Cell lawns were resuspended using ~5 mL of warm LB and used to inoculate 2-L baffled Erlenmeyer flasks each containing 1

L of LB broth and 50 mg/mL kanamycin. Cultures were incubated at 37 °C with shaking at 220 rpm, until mid-log phase ($OD_{600} = 0.9$). Cultures were induced with 100 μM IPTG and incubated for 3 h at 37 °C with shaking at 220 rpm. Cells were harvested by centrifugation at 3,500 g and the supernatants decanted. Cell pellets were resuspended in 100 mL ice-cold 50 mM HEPES/HCl, pH 7.5 and lysed by sonication for 12 min at 40 W using a Branson sonifier. The sonicate was centrifuged at 10,000 g for 45 min and the supernatant decanted and loaded at 1 mL/min onto a 10 mL BD Talon column pre-equilibrated with 50 mM HEPES/HCl, pH 7.5. A wash step of 200 mL at 1 mL/min was performed, the wash buffer consisting of 50 mM HEPES/HCl, 10 mM imidazole, pH 7.5. A 400 mL linear gradient from 10 to 300 mM imidazole in 50 mM HEPES/HCl, pH 7.5 was used to elute the protein that was collected as 5 mL fractions. A single symmetric peak was observed on the 280 nm chromatogram whose purity was subsequently verified by SDS-PAGE. Pure fractions were pooled and enzyme concentration was measured spectrophotometrically based on the measured extinction coefficient of the flavin at 464 nm (10,300 $M^{-1}cm^{-1}$). Total yields were routinely 6 mg/L. Imidazole was removed by 100,000-fold buffer exchange into 20 mM HEPES/HCl, pH 7.5 and concentrated using 10 kDa cutoff centrifugal-filters for storage at −80 °C.

A sample of ScOYE-3 (44 μM) was made anerobic as described above and mounted onto the quench instrument. A substrate sample containing NADH (200 μM) and a quench solution containing 1 M TCA and 1 mM EDTA were made anaerobic by sparging and loaded onto the instrument. The substrate solution also contained 300 μM tryptophan, which served as an inert internal standard. The enzyme and substrate samples were mixed and reacted for varied times (0.01–1000 s) before being quenched with the acid solution. The experiment was also performed aerobically as a positive control. The samples were retrieved from the instrument, incubated on ice for 15 min, and the precipitated protein was removed via centrifugation. The samples were analyzed via HPLC using the method described above for the single turnover EcDPD reaction.

Aerobically, complete consumption of the available NADH was observed, as the enzyme was able to perform multiple turnovers using molecular oxygen as the oxidant. However, it was found that scrubbing the system with a 1 mM glucose and 1 U/mL glucose oxidase solution for a minimum of 4 h before the start of the experiment was sufficient to remove ostensibly all of the oxygen from the system. As described above, there is added complexity to maintaining anaerobiosis resulting from the exposed purge and waste lines, as well as from the port that opens to the atmosphere to allow for sample collection. Because of this, the purge line was kept attached to a 50 mL gas-tight syringe filled with anaerobic scrubbing solution (buffered 1 mM glucose and 1 U/mL glucose oxidase) and was used to wash the entire system after each shot. 5 mL of this solution was used to flush across the mixing block, and 5 mL of solution was used to flush the age loop, quench loop, and waste line. The scrubbing solution was allowed to sit for a minimum of 5 min and a maximum of 10 min between each age time. Using this method, it was demonstrated that the amount of NADH consumed by ScOYE-3 was equal to the enzyme concentration and the consumption proceeded with the expected rate (determined previously by spectrophotometric methods). This indicates that the system was able to maintain anaerobiosis for the duration of the experiment, and that the method is suitable for studying reactions with significant oxygen reactivity.

3. Results and discussion

3.1. Predicted structure

While the mammalian and *E. coli* forms of DPD have the same cofactors, the mammalian enzyme is coded for by a single large gene and forms a functional homodimer, the bacterial enzyme is encoded by two genes that express to yield subunits that together form the equivalent of a single subunit of the mammalian form. As such, EcDPD is predicted to be a dimer of heterodimers. Fig. 1 compares the AlphaFold predicted structure of *E. coli* DPD with the known structure of porcine DPD [17]. A number of factors suggest the validity of the predicted fold, not least of which is that the 16 cysteine residues that are required to coordinate to the four Fe_4S_4 centers all position proximal to the clusters when the mammalian cofactors are aligned into the predicted bacterial structure. One curious difference from the mammalian enzyme is that the Fe_4S_4 center most proximal to the FAD cofactor is apparently coordinated conventionally with four cysteines, where the positionally equivalent cluster in the mammalian enzyme has three cysteines and one glutamine (Q156 in porcine DPD), indicating that this feature may not be unique to the chemistry catalyzed.

3.2. Expression and quantitation

DPD from *E. coli* was cloned in and expressed from the pETDuet-1 plasmid that provides independent expression of both genes that code for the enzyme. The yield of active enzyme was typically ~2 mg per liter of culture and could be stored at −80 °C without significant loss of activity. Furthermore, and contrary to prior reports, EcDPD can be purified under aerobic conditions and is stable for extended periods in air [10]. The cofactor composition of EcDPD was determined for the flavins by HPLC and this was correlated with the total iron content detected using an Fe(II) specific chelator. These data indicated a ratio of FAD:FMN:Fe of 1:0.92:16.6 ([FAD] = 21.4 ± 0.2 μM: [FMN] = 19.6 ± 0.4 μM: [Fe] = 356 ± 23 μM) consistent with the predicted cofactor set of FAD•4(Fe_4S_4)•FMN. The flavin determination method uses a denaturing surfactant, reductants, and EDTA to liberate the flavins and eliminate the chromophoric contributions of the iron-sulfur centers. As such the extinction coefficient of the as-isolated enzyme can be based on the known cumulative absorption contribution of both flavins and was found to be 71,000 $M^{-1}cm^{-1}$ at 445 nm, ostensibly the same as that determined for the mammalian form (75,000 $M^{-1}cm^{-1}$ at 426 nm) [5,

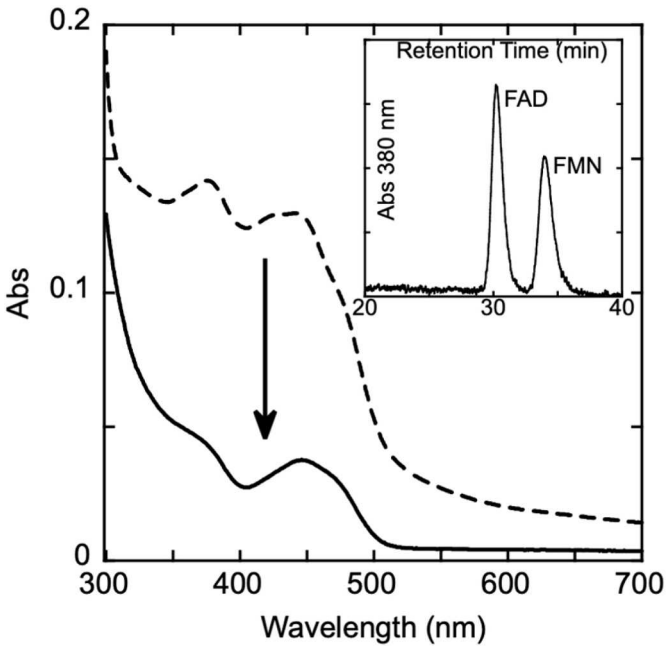

Fig. 2. Quantitation of the Flavin Content of EcDPD. A UV–Vis spectrum was measured for a sample of EcDPD (dashed line), and the sample was subsequently incubated at 70 °C for 1 h in the presence of 0.2 % SDS, 2 mM BME and 5 mM EDTA (solid line). The arrow indicates the loss of absorption from the iron sulfur centers. The sample was then analyzed for flavin content using HPLC and compared to standard curves for each flavin. The flavin content was then correlated with the measured iron content to determine the extinction coefficient spectrum of the enzyme.

21](Fig. 2).

3.3. Steady-state kinetic analysis

Steady-state kinetic measurements of EcDPD were undertaken under aerobic and anaerobic conditions. These data show that the kinetic parameters with both uracil and thymine are similar ($k_{catU} = 1.9 \pm 0.2\ s^{-1}$, $k_{cat}/K_{MU} = 25{,}600 \pm 400\ M^{-1}s^{-1}$, $k_{catT} = 1.6 \pm 0.1\ s^{-1}$, $k_{cat}/K_{MT} = 21{,}300 \pm 200\ M^{-1}s^{-1}$). Given that thymine is relatively deactivated for hydride transfer [9,22], these data imply that hydride transfer to the pyrimidine is not rate limiting for turnover in this form of the enzyme. Aerobic measurements indicate significant NADH oxidase activity resulting in turnover numbers that overestimate the rate of turnover by two-fold (Fig. 3A). With respect to NADH, the steady-state data indicate approximately ten-fold higher k_{cat}/K_M than observed for the pyrimidine substrates ($k_{cat}/K_{MNADH} = 2.17 \times 10^5 \pm 1.3 \times 10^4\ M^{-1}s^{-1}$) (Fig. 3B). When measured with dioxygen as the oxidant, the rate of NADH oxidation is approximately 70 % the rate observed with uracil as the oxidant indicating that valid steady-state measurements for either type of substrate can only be made under anaerobic conditions.

3.4. Dissociation constants for pyrimidine substrates

Titration of pyrimidine substrates to the oxidized form of DPD result in minor perturbations of the UV–Vis spectrum. These changes in absorbance are assumed to report progressive fractional saturation of the pyrimidine binding site adjacent to the FMN cofactor. EcDPD is prone to denature when incubated with substrate ligands in the absence of catalytic turnover. While limiting the time in incubation permitted the measurement of dissociation constants for uracil and thymine, NAD^+ induced denaturation even at modest concentrations and short incubation times. NADH reduces EcDPD and so the binding constant for this ligand was determined kinetically, see below. The measured dissociation constants for uracil and thymine were 9.7 ± 2.0 and 14.9 ± 1.0 μM respectively with difference spectra that closely resemble those observed with mammalian DPD (Fig. 4) [1]. The dissociation constants were used to define saturating conditions in transient state experiments by solving the quadratic form of the single site binding equation for fractional enzyme•ligand complex.

3.5. Transient state analysis of the reductive half-reaction

In the presence of NADH alone, EcDPD undergoes rapid reduction

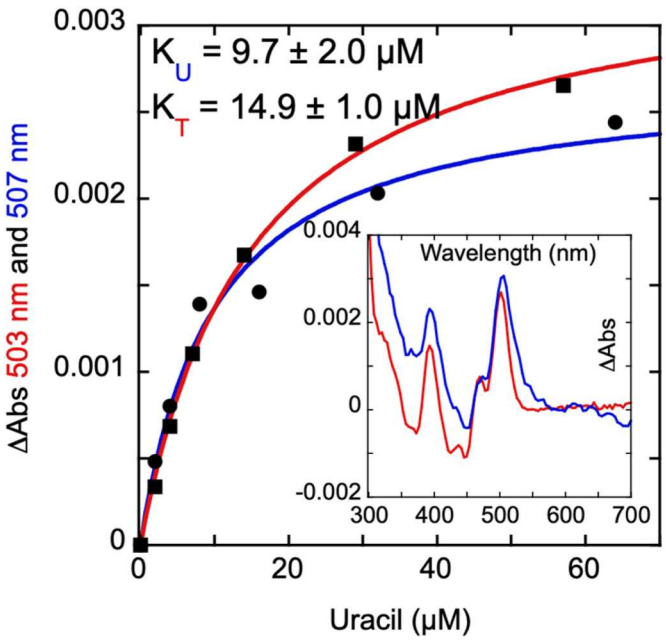

Fig. 4. Dissociation Constant Determinations for Substrate Pyrimidines. The dissociation constant for thymine (indicated in red) was determined by adding varied concentrations of thymine (2–57 μM) to individual 867 nM EcDPD samples and measuring the spectrum for each. Similarly, the dissociation constant for uracil (indicated in blue) was determined by adding varied concentrations of uracil (2–64 μM) to individual 944 nM EcDPD samples and measuring the spectrum for each. The changes in absorption were fit to Equation (3) to determine the dissociation constant. Inset depicts the difference binding spectra for the highest concentration of each ligand.

(Fig. 5). This differs from the mammalian enzyme, which only takes up electrons from NADPH at catalytically relevant rates in the presence of pyrimidine substrates [1]. When mixed with NADH under anaerobic conditions a multiphasic decrease in absorption is observed. Broadly, an initial rapid decrease precedes a second decrease that becomes more prominent at higher concentrations. A much slower decrease is also observed though this phase was not captured significantly in the data collected to 10 s. The data were best described when fit to a linear combination of three exponential terms according to Equation (4). However, the third phase is small and slow relative to the first two

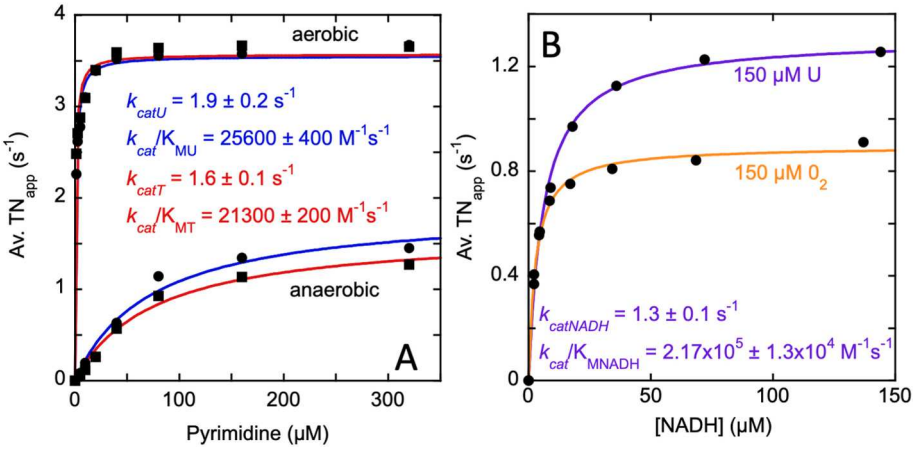

Fig. 3. Steady-state analysis of EcDPD. A. Aerobic vs anaerobic Michaelis-Menten analyses for uracil and thymine. Aerobic assays were undertaken with 710 nM EcDPD with varied thymine (■, red fit line) and uracil (●, blue fit line) concentration (1.25–320 μM) in the presence of 50 μM NADH. Anaerobic assays were undertaken with 990 nM EcDPD with varied thymine (■, red fit line) and uracil (●, blue fit line) concentration (5–320 μM) in the presence of 100 μM NADH. **B.** Michaelis-Menten analysis with varied NADH in the presence of uracil (●, purple fit line) (150 μM) and molecular oxygen (●, orange fit line) (150 μM). All data were fit to the Michaelis-Menten equation (Equations (1) and (2)).

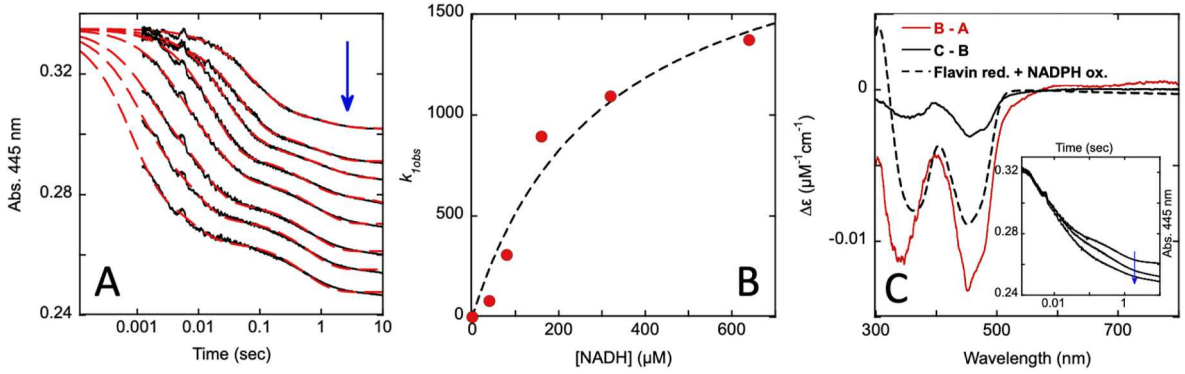

Fig. 5. Reductive Half Reaction. A. 4.7 μM EcDPD was mixed with varied concentrations of NADH (5, 10, 20, 40, 80, 160, 320, 640 μM) under anaerobic conditions (the arrow indicates increasing NADH concentration). The reduction of the enzyme was observed at 445 nm for two time frames (0.0012–0.2 s and 0.0012–10 s) and spliced together at the limit of the shorter. The data obtained (black traces) were fit (red dashes lines) to a linear combination of three exponentials according to Equation (4) assuming a common time zero absorbance. **B**. The dependence of the first observed rate constant determined in A plotted versus the NADH concentration fit to a single site binding equation according to Equation (5). **C**. 14.8 μM EcDPD was mixed with 76 μM NADH under anaerobic conditions and observed using charge coupled device detection for two time frames (0.0016–1.56 s and 0.0016–10 s) and spliced at the limit of the shorter. The data obtained were fit to a three species, two-step irreversible mechanism (A- > B- > C) and deconvoluted to yield spectra for each state (A, B, C). The spectra were then substracted to show the absorption changes that occur in each phase. Overlaid is the additive spectrum for flavin reduction and NADH oxidation (Flavin red. + NADH ox.) Inset: Suppression of the second phase using dihydrouracil (DHU). 4.7 μM EcDPD was mixed with 101 μM NADH with 0, 125, or 500 μM DHU and observed at 445 nm (the arrow indicates increasing DHU concentration).

phases and does not come to completion within the window of observation. As such the third term was included only to provide an improved measure of the first two phases. The observed rate constants for the first rapid phase for pseudo-first order reactant ratios were plotted against the concentration of NADH and fit to a hyperbolic function (Equation (5)) to determine the limiting rate of reduction as ~2,100 ± 450 s^{-1} and a poorly defined dissociation constant for NADH of 300 ± 140 μM. The amplitude of the first phase increases as the NADH concentration increases and does not appear to have reached a limit at ~140-fold the enzyme concentration. The second event that is more prominent at higher NADH concentrations is orders of magnitude slower and fit to a narrow range of observed rate constants (0.7–1.8 s^{-1}).

The reductive half reaction was also observed using CCD detection using an NADH concentration that was sufficiently high to resolve the two primary absorption decreases and provide pseudo-first order conditions such that the SVD fit to a two-step irreversible model returned spectra for the three states observed. The model-free singular value decomposition analysis indicated five species with two resembling noise. As such, the three-dimensional dataset was fit to a linear two-step irreversible model such that it reports the spectra for three reaction species. These spectra were then subtracted to define the changes occurring in each phase (Fig. 5C). These data show difference spectra consistent with NADH oxidation added to flavin reduction. The computed extinction coefficient change at 450 nm for the first phase is roughly consistent with the reduction of 1.5 flavins per subunit (based on a typical extinction coefficient change of 9,000 $M^{-1}cm^{-1}$ as indicated), suggesting that EcDPD can be reduced beyond the limit of two electrons observed with the mammalian enzyme. Given that we have no means to distinguish between FMN and FAD absorption transitions, these data do not define where the electrons acquired reside, however the data do indicate that there is no clear evidence of accumulated reduction of Fe_4S_4 centers. At wavelengths beyond 500 nm small broad increases in absorption are observed that presumably are charge transfer arising either from proximity of the NADH nicotinamide ring with the FAD isoalloxazine or from the converse oxidation states of either (see below). The absorption changes associated with the second phase are also indicative of flavin reduction, however the extinction coefficient change is consistent with ~0.35 flavins. As indicated in Fig. 5A, this feature becomes more prominent at higher concentrations resulting in increased net flavin reduction. When normalized at 445 nm the long wavelength transitions are superimposable for both difference spectra. A potential explanation is that electron transfer across the iron-sulfur centers is rapid and the FAD and FMN share a distribution of electrons that is defined by their individual reduction potentials such that the difference spectrum in terms of relative intensity of absorption transitions is the same in both reduction phases.

The origin of the second flavin reduction phase was investigated by repeating the reductive half reaction experiment at a single concentration of NADH and varied concentrations of DHU (Fig. 5C). The purpose was to assess if DHU that binds adjacent to the FMN could suppress this process, suggesting that the additional slow flavin reduction by NADH is occurring at the FMN site. The data show that the added flavin reduction phase can be eliminated by the addition of DHU (Fig. 5C inset) and therefore NADH can reduce EcDPD at either the FAD or the FMN, though the latter is only a significant factor at high NADH concentrations. The endpoints for this data presumably move to lower values as the total net reductants in the system increase with the addition of DHU. The AlphaFold prediction for EcDPD shown in Fig. 1 has the FMN bound to a domain that has a TIM-barrel topology. This domain is common to flavoproteins that bind pyrimidines for hydride transfer chemistry, specifically mammalian DPDs and dihydroorotate dehydrogenases (DHOD) [16,23,24]. In particular, class 1a DHOD is formed from only this fold and accomplishes its chemistry via a ping-pong kinetic mechanism with an intervening reduced state of the flavin that reduces NAD^+. The data above indicate that NADH has vestigial binding to the FMN domain of EcDPD and based on the conclusion above, these additional electrons redistribute between both flavins yielding a difference spectrum for the second reduction phase that is superimposable with that of the first reduction phase (Fig. 5C).

3.6. *Absorption changes in transient-state single turnover*

EcDPD was mixed under anaerobic conditions with saturating pyrimidines and limiting NADH with respect to the enzyme concentration. This approach has no certainty of approximating first-order conditions as the dissociation constant for NADH binding to the NADH•EcDPD•Pyr complex is not known, and the data above suggest binding is weak. Nonetheless, single wavelength data were acquired at 340 and 445 nm for uracil and thymine and fit analytically using a linear combination of exponential terms (Fig. 6). The fits obtained therefore report observed rate constants and are only useful descriptively. The data acquired for both uracil and thymine are very similar, suggesting that hydride

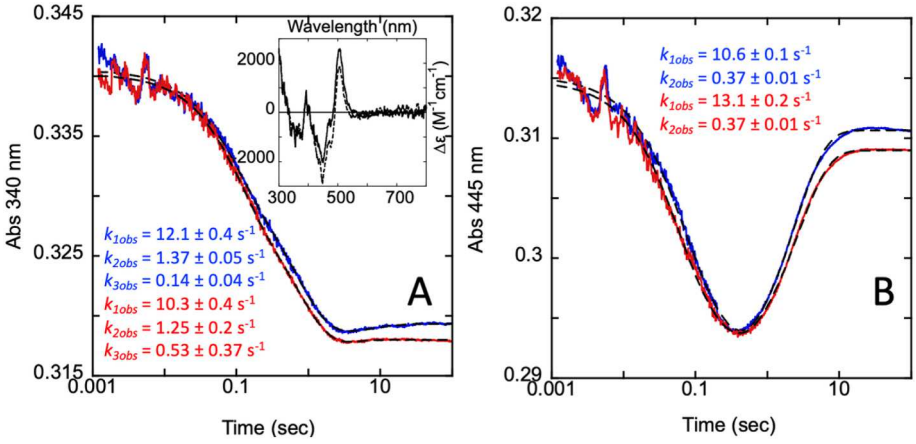

Fig. 6. Net Single Turnover with Limiting NADH. A. 4.6 μM EcDPD was mixed with 3.5 μM NADH and 200 μM uracil (blue) or thymine (red) under anaerobic conditions and observed at 340 nm. **B.** 4.6 μM EcDPD was mixed with 3.3 μM NADH and 200 μM uracil (blue) or thymine (red) under anaerobic conditions and observed at 445 nm. For **A.**, the 340 nm data were fit analytically to three exponentials. For **B.**, the 445 nm data were fit analytically to two exponentials. The rate constants obtained are as shown. The inset in **A.** shows the net absorption changes that occur with single turnover. For reference, the solid line was obtained by subtracting the spectrum obtained when 7.4 μM EcDPD was mixed with buffer from the spectrum obtained when mixed with 200 μM uracil. The dashed spectrum was when 7.8 μM EcDPD was mixed with 6.1 μM NADH and 200 μM Uracil under anaerobic conditions and the reaction observed using CCD detection. This spectrum was the difference of the unreacted enzyme mixed with buffer subtracted from the end-point spectrum obtained for the data shown in Fig. 7.

transfer to the pyrimidine is not markedly limiting in any phase observed. At 340 nm a decrease in absorption is observed reporting both oxidation of NADH and reduction of the enzyme. The data were fit to three exponentials with rate constants of ~11 s^{-1}, ~1.3 s^{-1} and ~0.1–0.5 (Fig. 6A). While the ~1.3 s^{-1} correlates well with the measured turnover number (Fig. 3), the value has uncertainty as the event prior is poorly delineated from it. The data acquired at 445 nm report only changes in the enzyme spectrum during single turnover. These show a decrease followed by an increase consistent with reduction and reoxidation of enzyme cofactors. Interestingly, the fit to two exponential phases returns observed rate constants of ~12 s^{-1} and ~0.4 s^{-1}, and the latter of which is three-fold slower than the rate of turnover.

Subtracting the t-zero spectrum measured prior to mixing with substrates from the spectrum of the enzyme at the end of turnover yields a difference spectrum that coincides with that for pyrimidine substrate binding (compare Fig. 4 inset, Fig. 6A inset). This indicates that the difference in amplitude for what are presumably successive reductive and oxidative phases arises from additive perturbation of the FMN spectrum with rebinding of pyrimidine substrates at the end of turnover.

Fig. 7 depicts the net absorption changes in each phase observed in single turnover limited by NADH concentration relative to the PreA:PreT concentration. These difference spectra were obtained by mixing EcDPD with limiting NADH in the presence of saturating uracil (95 %) or thymine (93 %) under anaerobic conditions and the reaction observed using CCD detection. Spectra for individual transients were obtained by singular value decomposition of datasets containing time-resolved absorption spectra. The datasets were fit to a linear three-step irreversible model returning rate constants of 22.2 ± 0.4 s-1, 1.5 ± 0.1 s^{-1} and 0.65 ± 0.02 s^{-1} for uracil and 23.4 ± 0.6 s-1, 3.4 ± 0.2 s^{-1} and 0.76 ± 0.02 s^{-1} for thymine. The deconvoluted spectra were then subtracted in successive pairs to yield the net absorption changes in each phase observed.

The difference spectra obtained indicate that the uracil and thymine reactions are very similar. The changes observed in the first phase (red difference spectrum) show evidence for simultaneous NADH oxidation and flavin reduction. The extinction coefficient changes for this phase

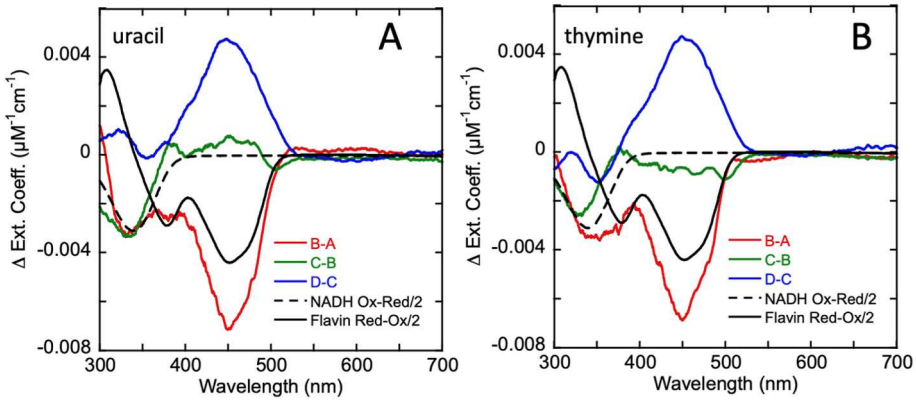

Fig. 7. Spectral Deconvolution of EcDPD Single Turnover Reactions. 7.8 μM EcDPD was mixed with 6.1 μM NADH and 200 μM uracil (**A**) or 200 μM thymine (**B**) under anaerobic conditions and the reaction observed using CCD detection. The spectra shown were obtained by singular value decomposition of datasets containing time-resolved absorption spectra. In each case data were collected for two time frames (0.0016–1.6 s and 0.0016–15.7 s) and the data spliced together at the limit of the earlier dataset. The composite dataset was fit to a linear three-step irreversible model returning rate constants of 22.2 ± 0.4 s^{-1}, 1.5 ± 0.1 s^{-1} and 0.65 ± 0.02 s^{-1} for uracil and 23.4 ± 0.6 s^{-1}, 3.4 ± 0.2 s^{-1} and 0.76 ± 0.02 s^{-1} for thymine. The difference spectra shown in **A** & **B** were obtained by subtracting successive spectrum pairs such that they report the net absorption changes in each phase and have the sequence progression of red (1), green (2) and blue (3) lines. Each has overlayed reference difference spectra for one half equivalent of flavin reduction (solid black) and NADH oxidation (dashed black) relative to the PreA:PreT concentration.

are approximately equal to 0.8 flavins reduced and 0.5 NADH oxidized per PreA:PreT. While the spectra faithfully report what is occurring in terms of substrate/cofactor engagement, discrepancies in extinction coefficient changes are likely a result of a lack of delineation between the first and second phases (as mentioned above for Fig. 6) resulting in error in the rate constants derived from the fit and consequent distortion of the deconvoluted spectra. Nonetheless, the data are consistent with reductive activation in which two electrons are taken up to reduce one of the two flavins in the PreA:PreT dimer. The second phase shows primarily evidence of NADH oxidation (green difference spectrum) equivalent to 0.5 of the PreA:PreT concentration. This subsequent NADH oxidation is consistent with pyrimidine reduction and given that no further flavin reduction is observed, that the NADH is oxidized to maintain the enzymes oxidation state, much as was observed for the mammalian enzyme [25]. However, both datasets fit to include a rate constant slower than the measured rate of turnover. The phase associated with this rate constant has spectral changes indicative of flavin reoxidation (blue difference spectrum). The magnitude of this phase mirrors flavin reduction observed in the first phase and therefore must return the enzyme to its initial oxidation state with both flavins oxidized. Given that this event is slower than the limiting rate of catalysis, it is assigned as a secondary phase of pyrimidine reduction where electrons acquired in activation are slowly lost to the excess oxidant substrate pool in the absence of NADH. This behavior is distinct from the reductively activated mammalian enzyme that shows no evidence of pyrimidine reduction in the absence of NADPH. So, EcDPD also requires NADH bound at the FAD site to promote pyrimidine reduction at the FMN site at catalytically relevant rates indicating intersubunit (PreA-PreT) communication, but, unlike the mammalian enzyme, can offload electrons acquired in reductive activation to the pyrimidine in the absence of NADH. The data also show no distinct evidence of iron-sulfur center reduction. This indicates that electrons span the distance between the FAD and FMN rapidly such that no evidence of flavin semiquinone or reduced iron-sulfur centers are observed to accumulate.

3.7. Rapid mixing acid quench

Meaningful assignment of the three phases observed in single turnover transient state spectrophotometric experiments is contingent on time-resolved product analysis to show how substrates and products decay and accumulate with time. Single turnover experiments were repeated using a rapid mixing chemical quench instrument. EcDPD was mixed with limiting NADH and saturating thymine and quenched at various times using acid and EDTA. The aged and quenched samples were analyzed for concentrations of reactants and products. Partial cyclization of NADH under acidic conditions dictated that NAD^+ be quantified to track oxidation of NADH. Though saturating and in relative high concentration, thymine was used to quantify reaction progress for the pyrimidine substrate. Dihydrothymine has at low extinction coefficient and absorbs light only at short wavelengths, complicating its accurate quantitation. Fig. 8 shows reduction of thymine and oxidation of NADH observed by rapid quench. The figure depicts the concentration profile expected for a three-step irreversible reaction based on the measured rate constants (see Fig. 7) and concentrations used. The degree of scatter in this data precludes fitting for rate constant determination and the data were overlaid with lines that illustrate the expected accumulation or decay of each substance tracked by this method based on rate constants measured in other experiments.

The data for thymine and NAD^+ are displaced in time but mirrored in terms of amplitude, definitively establishing that all electrons derived from NADH are passed to thymine during the span of the observation. The data qualitatively conform to equal concentrations of NADH being oxidized in the first and second events (23.4 s^{-1} and 3.4 s^{-1}) and equal concentrations of thymine being reduced in the second and third events (3.4 s^{-1} and 0.76 s^{-1}). If so, this implies that the third phase in which only thymine is reduced occurs as NADH is depleted in the presence of an excess of the pyrimidine substrate. Given that this phase returns the enzyme to its fully oxidized state (Fig. 7) this process ensures that all electrons that enter the enzyme from NADH are delivered to the pyrimidine. Both illustrative lines included in Fig. 8 have fixed and equal changes in concentration in both phases. The smaller degree of scatter and the 7-fold difference in rate constant make this ratio more apparent for NAD^+ quantitation. Each phase consumes an amount of NADH equal to one half the heterodimer (PreA-PreT) concentration. This indicates that EcDPD displays half-of-sites activity where one heterodimer pair is reductively activated and then subsequently reduces pyrimidine, as was observed for the mammalian enzyme [1].

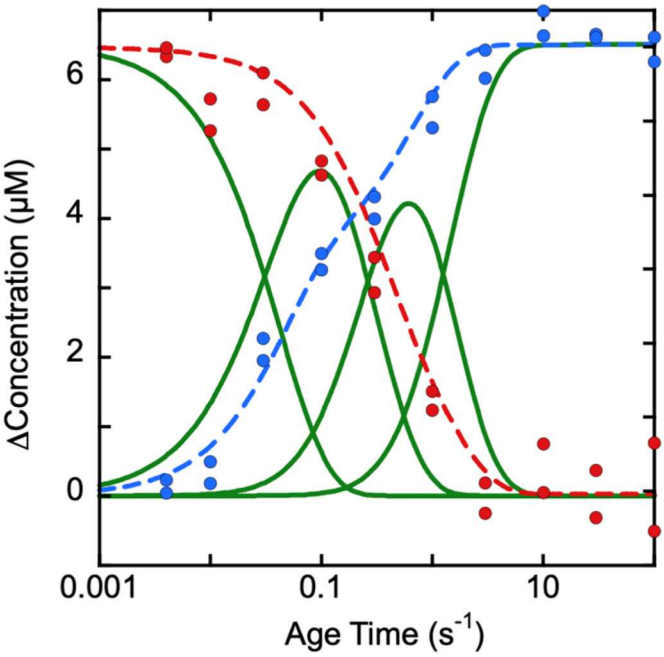

Fig. 8. Rapid Chemical Quench of EcDPD Single Turnover Reactions. 6.5 μM EcDPD was mixed with 6.5 μM NADH and 150 μM thymine under anaerobic conditions. Each reaction was aged for the times indicated and quenched with 500 mM trichloroacetic acid, 0.5 mM EDTA. The data track thymine reduction (red) and NAD^+ accumulation (blue). Green lines indicate the predicted species concentration profile for an irreversible linear kinetic sequence with rate constants of 23.4 s^{-1}, 3.4 s^{-1} and 0.76 s^{-1}. The data shown has overlaid dashed lines that illustrate the line shapes expected for these rate constants (Fig. 7). For NAD^+ accumulation the overlaid line is formed from rate constants of 23.4 s^{-1}, 3.4 s^{-1} with equal concentration accumulating in both phases. The line overlaid for reduction of thymine depicts expectation for rate constants of 3.4 s^{-1} and 0.76 s^{-1} and an equal concentration reduced in both phases.

4. Conclusions

Mechanistically, EcDPD exhibits a variation of what was observed for the mammalian DPD enzyme. Structural prediction suggests that the overall structure of both forms of the enzyme is similar. Both undergo reductive activation prior to pyrimidine reduction and in the mammalian enzyme it was established that the two electrons acquired reside on the FMN cofactor [8]. Difference spectra derived from single turnover reactions with both enzymes include no evidence of iron-sulfur center reduction indicating that electron transmittance across the enzyme is fast relative to chemistry that occurs with the substrates and products.

When comparing Fig. 8 to the data depicted in Fig. 3A and 7 distinct functional conclusions can be drawn for EcDPD. The quench data are consistent with a model in which EcDPD takes up two electrons to reductively activate in a similar manner to that observed with the mammalian enzyme. However, EcDPD takes up electrons rapidly in the absence of the pyrimidine substrate suggesting that the stimulatory

effector role for the pyrimidine in reductive activation observed with mammalian DPD is not built into activation of the bacterial enzyme. Stoichiometry indicates half-of-sites activity in which one PreT, PreA dimer is engaged in the presence of limiting NADH with respect to the enzyme concentration. These electrons can then be passed to the pyrimidine substrate, but two avenues are available for this to occur. In the presence of NADH the pyrimidine is reduced more rapidly (1.5–3.4 s^{-1}) and NADH can restore the activated oxidation state with each turnover. For this reason, the turnover number measured in the presence of excess substrates more closely matches rate of pyrimidine reduction in turnover. In the absence of NADH the electrons depart the enzyme to reduce pyrimidine more slowly (0.5–0.7 s^{-1}). This occurs in stark contrast to the mammalian DPD enzyme that retains two electrons when NADPH is exhausted and will not reoxidize in the presence of oxidant pyrimidine substrate [1]. For EcDPD, excess pyrimidine can draw out electrons used to (re)activate the enzyme returning the enzyme to the FAD•4(Fe_4S_4)• FMN state.

The reasons for the mechanistic differences between the *E. coli* and pig DPDs cannot be established from the data presented. For mammalian DPD the effector role for NADPH in pyrimidine reduction ensures reductive reactivation of the enzyme and thereby completes the catalytic cycle. For the *E. coli* enzyme, a similar objective is achieved but via specific reoxidation of the enzyme by pyrimidines. Both mechanisms ensure that electrons acquired are committed to the specific chemistry catalyzed. It is difficult to imagine an *in vivo* circumstance where either of the observed oxidative mechanisms becomes relevant given that they are only revealed as distinct from one another when the reductant substrate is exhausted, and these molecules are generally maintained at relatively constant concentrations of 10–20 μM (NADPH) in mammalian cells [26] and ~80 μM (NADH) in *E. coli* cells [27].

Acknowledgements

This research was supported by National Science Foundation Grant CHE 2203593 to G.R.M.

References

[1] B.A. Beaupre, D.C. Forouzesh, G.R. Moran, Transient-state analysis of porcine dihydropyrimidine dehydrogenase reveals reductive activation by NADPH, Biochemistry 59 (2020) 2419–2431.
[2] D. Dobritzsch, G. Schneider, K.D. Schnackerz, Y. Lindqvist, Crystal structure of dihydropyrimidine dehydrogenase, a major determinant of the pharmacokinetics of the anti-cancer drug 5-fluorouracil, EMBO J. 20 (2001) 650–660.
[3] D. Dobritzsch, K. Persson, G. Schneider, Y. Lindqvist, Crystallization and preliminary X-ray study of pig liver dihydropyrimidine dehydrogenase, Acta Crystallogr D Biol Crystallogr 57 (2001) 153–155.
[4] K. Rosenbaum, K. Jahnke, K.D. Schnackerz, P.F. Cook, Secondary tritium and solvent deuterium isotope effects as a probe of the reaction catalyzed by porcine recombinant dihydropyrimidine dehydrogenase, Biochemistry 37 (1998) 9156–9159.
[5] K. Rosenbaum, K. Jahnke, B. Curti, W.R. Hagen, K.D. Schnackerz, M.A. Vanoni, Porcine recombinant dihydropyrimidine dehydrogenase: comparison of the spectroscopic and catalytic properties of the wild-type and C671A mutant enzymes, Biochemistry 37 (1998) 17598–17609.
[6] K. Rosenbaum, B. Schaffrath, W.R. Hagen, K. Jahnke, F.J. Gonzalez, P.F. Cook, K. D. Schnackerz, Purification, characterization, and kinetics of porcine recombinant dihydropyrimidine dehydrogenase, Protein Expr. Purif. 10 (1997) 185–191.
[7] D.J. Porter, T. Spector, Dihydropyrimidine dehydrogenase. Kinetic mechanism for reduction of uracil by NADPH, J. Biol. Chem. 268 (1993) 19321–19327.
[8] B.A. Beaupre, D.C. Forouzesh, A. Butrin, D. Liu, G.R. Moran, Perturbing the movement of hydrogens to delineate and assign events in the reductive activation and turnover of porcine dihydropyrimidine dehydrogenase, Biochemistry 60 (2021) 1764–1775.
[9] M.M. Smith, D.C. Forouzesh, N.E. Kaley, D. Liu, G.R. Moran, Mammalian Dihydropyrimidine Dehydrogenase: Answers to Outstanding Mechanistic Questions from Transient State Analysis of Charge Transfer Complexes, Archives of Biochemistry and Biophysics in press, 2023.
[10] H. Yoshioka, T. Ishida, H. Mihara, Overexpression and characterization of Escherichia coli dihydropyrimidine dehydrogenase, a four iron-sulfur cluster containing flavoprotein, J. Biochem. 170 (2021) 511–520.
[11] J.M. Ploeser, H.S. Loring, The ultraviolet absorption spectra of the pyrimidine ribonucleosides and ribonucleotides, J. Biol. Chem. 178 (1949) 431–437.
[12] P.O.P. Ts'o, I.S. Melvin, A.C. Olson, Interaction and association of bases and nucleosides in aqueous solutions, J. Am. Chem. Soc. 85 (1963) 1289–1296.
[13] A.D. Winer, Crystallization of nicotinamide adenine dinucleotide, J. Biol. Chem. 239 (1964) PC3598+.
[14] B.L. Horecker, A. Kornberg, The extinction coefficients of the reduced band of pyridine nucleotides, J. Biol. Chem. 175 (1948) 385–390.
[15] R.M. Kohli, V. Massey, The oxidative half-reaction of Old Yellow Enzyme. The role of tyrosine 196, J. Biol. Chem. 273 (1998) 32763–32770.
[16] K.D. Schnackerz, D. Dobritzsch, Y. Lindqvist, P.F. Cook, Dihydropyrimidine dehydrogenase: a flavoprotein with four iron-sulfur clusters, Biochim. Biophys. Acta 1701 (2004) 61–74.
[17] D. Dobritzsch, S. Ricagno, G. Schneider, K.D. Schnackerz, Y. Lindqvist, Crystal structure of the productive ternary complex of dihydropyrimidine dehydrogenase with NADPH and 5-iodouracil. Implications for mechanism of inhibition and electron transfer, J. Biol. Chem. 277 (2002) 13155–13166.
[18] M. Hedayati, B. Abubaker-Sharif, M. Khattab, A. Razavi, I. Mohammed, A. Nejad, M. Wabler, H. Zhou, J. Mihalic, C. Gruettner, T. DeWeese, R. Ivkov, An optimised spectrophotometric assay for convenient and accurate quantitation of intracellular iron from iron oxide nanoparticles, Int. J. Hyperther. 34 (2018) 373–381.
[19] F.E. Smith, J. Herbert, J. Gaudin, D.J. Hennessy, G.R. Reid, Serum iron determination using ferene triazine, Clin. Biochem. 17 (1984) 306–310.
[20] G.R. Moran, Anaerobic methods for the transient-state study of flavoproteins: the use of specialized glassware to define the concentration of dioxygen, Methods Enzymol. 620 (2019) 27–49.
[21] B.A. Beaupre, J.V. Roman, G.R. Moran, An improved method for the expression and purification of porcine dihydropyrimidine dehydrogenase, Protein Expr. Purif. 171 (2020), 105610.
[22] R.N. Goyal, U.P. Singh, A.A. Abdullah, Electrochemical oxidation of uracil and 5-halouracils at pyrolytic graphite electrode, Indian J. Chem. 42 (2003) 42–47.
[23] R.L. Fagan, K.F. Jensen, O. Bjornberg, B.A. Palfey, Mechanism of flavin reduction in the class 1A dihydroorotate dehydrogenase from Lactococcus lactis, Biochemistry 46 (2007) 4028–4036.
[24] R.L. Fagan, M.N. Nelson, P.M. Pagano, B.A. Palfey, Mechanism of flavin reduction in class 2 dihydroorotate dehydrogenases, Biochemistry 45 (2006) 14926–14932.
[25] M.M. Smith, G.R. Moran, The unusual chemical sequences of mammalian dihydropyrimidine dehydrogenase revealed by transient-state analysis, Methods Enzymol. 685 (2023) 373–403.
[26] T.G. Demarest, G.T.D. Truong, J. Lovett, J.G. Mohanty, J.A. Mattison, M. P. Mattson, L. Ferrucci, V.A. Bohr, R. Moaddel, Assessment of NAD(+)metabolism in human cell cultures, erythrocytes, cerebrospinal fluid and primate skeletal muscle, Anal. Biochem. 572 (2019) 1–8.
[27] B.D. Bennett, E.H. Kimball, M. Gao, R. Osterhout, S.J. Van Dien, J.D. Rabinowitz, Absolute metabolite concentrations and implied enzyme active site occupancy in Escherichia coli, Nat. Chem. Biol. 5 (2009) 593–599.